Article

Journal of the Brazilian Chemical Society

https://dx.doi.org/10.21577/0103-5053.20240093

J. Braz. Chem. Soc. **2024**, *35*, 11, e-20240093, 1-9

Evaluation of Nitrogen-Doped Adsorbents Based on Reduced Graphene Oxide as Platforms for CO_2 Capture

Matheus G. Ribeiro, [a] ***Isabela A. A. Bessa,*** [a] ***Aline F. M. da Silva,*** [a] ***Carolina B. P. Ligiero,*** [a] ***Leonardo O. Osta,*** [b] ***Ludmila P. C. Silva,*** [c] ***Joyce R. Araujo,*** [d] ***Bráulio S. Archanjo,*** [d] ***Célia M. Ronconi*** [a] ***and Thiago C. dos Santos*** *[,b]

[a]*Departamento de Química Inorgânica, Universidade Federal Fluminense, Campus do Valonguinho, Outeiro São João Batista s/n, Centro, 24020-150 Niterói-RJ, Brazil*

[b]*Instituto de Química, Universidade Federal do Rio de Janeiro. Av. Athos da Silveira Ramos 149, CT, Cidade Universitária, 21941-909 Rio de Janeiro-RJ, Brazil*

[c]*Departamento de Engenharia Química e Petróleo, Universidade Federal Fluminense, Campus da Praia Vermelha, R. Passo da Pátria 152-470, São Domingos, 24210-240 Niterói-RJ, Brazil*

[d]*Divisão de Metrologia de Materiais, Instituto Nacional de Metrologia, Qualidade e Tecnologia (Inmetro), 25250-020 Duque de Caxias-RJ, Brazil*

CO_2 emissions into the atmosphere have been rapidly rising due to human activities, resulting in the escalation of global warming. To mitigate climate change, it is imperative to develop materials for CO_2 capture with high CO_2 capacity and low production costs. Herein, we developed a facile method to obtain adsorbents based on reduced graphene oxide (rGO) sheets, NrGO(1 – X)700, where X represents the mass of diethylenetriamine (DETA) (X = 1, 2 and 4 g) used in the preparation. The materials NrGO(1 – 1)700, NrGO (1 – 2)700, and NrGO(1 – 4)700 were obtained from graphene oxide dispersions, followed by DETA impregnation and chemical activation with K_2CO_3. N_2 isotherms demonstrated that the materials simultaneously presented micro and mesopores with similar values of specific surface area (280.16 to 310.32 $m^2\ g^{-1}$), pore volume (0.26 to 0.28 $cm^3\ g^{-1}$) and pore size (3.78 to 3.80 nm). CO_2 sorption experiments revealed that the material NrGO(1 – 4)700, containing the highest amount of pyridinic, graphitic, and amino nitrogen functionalities, showed the best CO_2 adsorption capacity. Diffuse reflectance Fourier transformed infrared spectroscopy experiments indicated stronger solid-gas interactions for NrGO(1 – 4)700 than for the other materials.

Keywords: CO_2 capture, porous materials, reduced graphene oxide, nitrogen-doped adsorbent

Introduction

In the last decades, the atmospheric CO_2 concentration has rapidly increased due to anthropogenic activities, e.g., fossil fuel combustion, forest fires and agricultural activities, resulting in climate changes.[1-3] CO_2 capture and storage is considered a short to medium-term strategy to mitigate CO_2 release.[4-6] In coal-fired power stations, CO_2 is removed from the flue gas stream by aqueous alkanolamines solutions, which is a costly technology.[7-9] Thus, porous solids represent an attractive technology for CO_2 capture due to their easy preparation, eco-friendliness, and low operation costs. A wide variety of adsorbents (including mesoporous silica, activated carbon, graphene-based porous adsorbents, zeolites, metal organic framework (MOFs) and porous covalent organic network (COFs))[10-20] has been extensively studied for remediation of toxic environmental pollutants, such as herbicide removal, extraction of heavy metal ions and CO_2 adsorption.[21-24] Among these solids, some exhibit low CO_2 adsorption, moisture intolerance, prolonged times to reach gas saturation due to low kinetic adsorption, complex syntheses, and weak mechanical properties. Therefore, there is an urgent need to develop new porous solids with advanced properties for application in CO_2 capture.

*e-mail: thiagocustodio@iq.ufrj.br
Editor handled this article: Aldo José Gorgatti Zarbin (Guest)
Dedicated to the memory of Prof Oswaldo Luiz Alves for his great contribution to the field of solid-state chemistry.

Graphene-based porous adsorbents are considered a next-generation solution due to the characteristics of graphene, which exhibits a large specific surface area (2630 $m^2\ g^{-1}$), high mechanical strength and thermal stability.[25-28] However, graphene sheets have a tendency to form irreversible agglomerates via π-π restacking, resulting in solids with inaccessible surface areas.[29,30] Several synthesis methods, including aerogel preparation,[31,32] self-assembly processes of sheets,[15] pillared graphene layers,[33,34] and chemical activation processes,[35] have been reported to improve the specific surface areas of the solids (170-1155 $m^2\ g^{-1}$).[36] However, for CO_2 adsorption, not only is a large specific surface area necessary, but also other physical (pore volume and pore size distribution) and chemical properties (presence of amino groups and nitrogen atoms) can influence the performance of the materials.[37] For example, microporous materials present sufficient solid-gas forces to trap CO_2 molecules at 1 bar and room temperature.[38] On the other hand, larger pore sizes (meso and macropores) do not exhibit considerable CO_2 adsorption under the same conditions due to weak solid-gas interactions.[39] Yang *et al.*[40] studied the kinetic of CO_2 adsorption on SBA-15 (mesoporous material) and activated carbon (micro, meso, and macroporous materials), demonstrating that permeability into the meso/macropores is 3-6 orders of magnitude larger than into the micropores. Therefore, interconnected pore architectures containing bimodal distributions are desirable for CO_2 capture due to the higher CO_2 capacity of micropores and facile permeability of mesopores. Additionally, the introduction of nitrogen atoms into mesoporous graphene can improve physical solid-gas interactions.[35] Another strategy is to introduce amino groups because they can react with CO_2 molecules, yielding carbamate species.[41]

In this work, we describe the fabrication of graphene oxide (GO) containing interconnected micro and mesopores, simultaneously functionalized with amino groups and doped with different types of nitrogen atoms (pyridine, graphitic, and pyrrole nitrogen). The solids were named NrGO(1 – X)700, where X = 1, 2, 4 g represents the mass of diethylenetriamine (DETA) added to the graphene oxide (1 g) water dispersion. The adsorbents NrGO(1 – X)700 were fabricated from GO dispersions and DETA, followed by an activation process with K_2CO_3. The material NrGO(1 – 4)700, prepared with the highest GO/DETA ratio (1:4), demonstrated the best CO_2 adsorption capacity. This performance was correlated with its highest percentage of amino group and graphic nitrogen.

Experimental

Chemicals

The chemicals employed in this work were purchased from Sigma-Aldrich (St. Louis, USA) and Vetec (Rio de Janeiro, Brazil) and used as received: graphite flakes (≥ 99%), phosphorus pentoxide (P_4O_{10}, ≥ 99%), sodium nitrate ($NaNO_3$, ≥ 99%), potassium permanganate ($KMnO_4$, 97%), chloridric acid (HCl, 35-37%), sulfuric acid (H_2SO_4, 98%), hydrogen peroxide (H_2O_2, ≥ 30%), methanol (MeOH, 99.8%), potassium carbonate (K_2CO_3, ≥ 99%) and diethylenetriamine (DETA) ($HN(CH_2CH_2NH_2)_2$, ≥ 98.5%). CO_2 (99.9%) was acquired from White Martins (Rio de Janeiro, Brazil), He (99.999%) and N_2 (99.999) were acquired from Tecgases (Rio de Janeiro, Brazil).

Syntheses of NrGO(1 – X)700 materials

The graphene oxide used to fabricate the NrGO(1 – X)700 was obtained by a method previously reported by our group,[42,43] and based on Hummer's method.[44] A dispersion of GO (1.0 g) in 250 mL of distilled water was sonicated for 120 min, resulting in a brown dispersion with a concentration of 4 $mg\ mL^{-1}$. Then, 30, 60 or 120 mL of DETA solution (33.3 $g\ L^{-1}$) were added dropwise to the GO dispersions and transferred to an autoclave (Parr 4748) of 100 mL, which was maintained under magnetic stirring during 24 h at 120 °C. The dispersion was freeze-dried for 2 days to yield NrGO(1 – X). Then, each solid was chemically activated with K_2CO_3 using a NrGO(1 – X):K_2CO_3 ratio of 1:1, where 1.0 g of NrGO(1 – X) was added to a methanolic solution of K_2CO_3 (1.0 g in 70 mL of MeOH). The dispersion was heated up to 70 °C, under magnetic stirring. After the methanol evaporation, the solids were heated up to 200 °C under an N_2 flow (100 $mL\ min^{-1}$) for 1 h in a horizontal furnace. Then, the temperature was raised to 700 °C and maintained for 2 h. After cooling to room temperature, the solids were washed using Milli-Q water until the pH reached 7.0 and dried at room temperature, yielding NrGO(1 – 1)700 (0.0882 g), NrGO(1 – 2)700 (0.0586 g) and NrGO(1 – 4)700 (0.0849 g). Elemental analyses (CHN) for NrGO(1 – 1)700 were: C, 75.04; H, 0.82; N, 5.09%; NrGO(1 – 2)700: C, 76.36; H, 0.95; N, 4.78%; NrGO(1 – 4)700: C, 76.68; H, 1.22; N, 5.39%.

Characterization techniques

Elemental analyses were performed using a PerkinElmer (Shelton, USA) model 240C series ii at the Analytical

Central IQ-USP. X-ray photoelectron spectroscopy (XPS) was conducted using a Scienta Omicron (Uppsala, Sweden) GmbH (10^{-7} Pa) system. All spectra were measured using a monochromatic Al Kα radiation source (hν = 1486.6 eV). High-resolution spectra were obtained with a pass energy (E_{pass}) of 30 eV, and the peaks were fitted using CasaXPS software.[45] Attenuated total reflectance with Fourier transform infrared (ATR-FTIR) spectra recorded from 400 to 4000 cm^{-1} on a Thermo Nicolet FTIR iS50 spectrometer (Waltham, USA). Raman spectra at 532 nm were acquired using a Witec Alpha 300R spectrometer (Ulm, Germany) equipped with a 50X objective lens. Powder X-ray diffraction (PXRD) patterns were obtained on a Miniflex-Rigaku (Tokyo, Japan) using a Cu Kα radiation of 1.5418 Å, generated at 30 kV and 15 mA. All data were acquired at room temperature over a 2θ range from 5 to 70°, in steps of 0.02°, and with a counting time of 1 s *per* step. Nitrogen isotherms, at −196 °C, were measured using ASAP 2020 Micromeritic (Norcross, USA) equipment, in the range of 0 to 1 bar. Specific surface areas were calculated using the Brunauer-Emmett-Teller (BET) equation, and pore size distributions were determined by the Barrett-Joyner-Halenda (BJH) method. Before the analyses, 100 mg of the sample was degassed at 120 °C for 48 h. Scanning electron microscopy (SEM) images were acquired with a Magellan 450 (FEI Company, Hillsboro, USA) microscope using an FEG source at 5 KeV and a current of 50 pA. Approximately 1 mg of each sample was dispersed in 3 mL of isopropanol and sonicated for 1 h. Then, 10 μL of the dispersion was dropped onto a silicon substrate and the solvent was allowed to evaporate under ambient conditions.

CO_2 studies

CO_2 isotherms were measured using ASAP 2020 (Norcross, USA) e-serial 1200 equipment at 25 °C, in the range of 0 to 1 bar. The materials (60 mg) were degassed at 120 °C for 24 h before the measurements. Diffuse reflectance Fourier transformed infrared spectroscopy (DRIFTS) experiments were conducted on a Bruker Vertex 70 spectrophotometer (Billerica, USA), equipped with a Harrick reflectance accessory, containing a reaction chamber (HVC-DRP-4, Harrick) and ZnSe windows. The samples were initially dried *in situ* at 100 °C under He flow for 15 min and then cooled to 30 °C, at which point the background interferogram was collected under He flow. Subsequently, the samples were exposed to a CO_2 flow for 15 min. After this, the stream was switched to He and a spectrum was immediately collected. At the end of this measurement (approximately 47 s), two minutes were allowed to pass before acquiring a new spectrum. This procedure was repeated nine more times (2-20 min). The interferograms were obtained after 256 scans at a resolution of 16 cm^{-1}.

Results and Discussion

Syntheses of materials

The adsorbents NrGO(1 – X)700 were prepared from GO and DETA, serving as carbon and nitrogen sources, respectively. Initially, mixtures of GO dispersion and DETA solutions were heated up to 120 °C in a Parr autoclave (hydrothermal procedure) to produce reduced graphene oxide platforms containing nitrogen atoms. Subsequently, these materials were annealed at 700 °C with K_2CO_3 under an N_2 flow to produce NrGO(1 – X)700, where X represents 1, 2 and 4 g of DETA. At high temperature, K_2CO_3 reacts with carbon layers of GO, enlarging the voids and removing carbon atoms.[46,47] These oxidation reactions produce CO and CO_2, creating holes in the carbon network (equations 1-3), and enhancing the specific surface area of the materials. Different amounts of DETA were used to evaluate the nitrogen contents and types incorporated into the adsorbents and to correlate them with the CO_2 adsorption capacities.

$$K_2CO_{3(s)} \rightarrow K_2O_{(s)} + CO_{2(g)} \quad (1)$$

$$C_{(s)} + CO_{2(g)} \rightarrow 2CO_{(g)} \quad (2)$$

$$K_2O_{(s)} + C_{(s)} \rightarrow 2K_{(s)} + CO_{(g)} \quad (3)$$

Characterizations

XPS survey spectra of NrGO(1 – X)700 are presented in Figures 1a-1c. The signals at 284.6, 531.6 and 398.6 eV were attributed to C 1s, O 1s and N 1s, respectively, confirming the presence of nitrogen atoms. The nitrogen content, derived from area integration of the N 1s peak was found to be 4.13, 3.43 and 5.58% for NrGO(1 – 1)700, NrGO(1 – 2)700 and NrGO(1 – 4)700, respectively. These findings are in agreement with the elemental analyses. High-resolution XPS spectra of N 1s, shown in Figures 1d-1f, were analyzed to identify the types of nitrogen moieties. The deconvolution of the signal at 398.6 eV (N 1s) revealed five new peaks centered at approximately 397.0, 398.1, 399.2, 400.3 and 402.5 eV. These correspond to pyridinic-N, amino, pyrrolic-N, graphitic-N and oxidized-N, respectively. These results confirmed that the nitrogen atoms were incorporated into reduced graphene oxide networks. The contributions of each nitrogen species are detailed in Table 1.

Table 1. Energies and nitrogen percentages determined by high-resolution XPS of N 1s

Material	Energy (N / %) / eV				
	Pyridinic-N	Amino	Pyrrolic-N	Graphitic-N	Oxidized-N
NrGO (1 – 1)700	397.0 (21.31)	398.3 (14.87)	399.3 (10.42)	400.5 (39.48)	402.9 (14.91)
NrGO (1 – 2)700	397.0 (33.27)	398.5 (18.88)	399.3 (6.17)	400.3 (26.40)	403.0 (15.28)
NrGO (1 – 4)700	397.0 (9.33)	398.1 (20.10)	399.2 (18.14)	400.3 (41.32)	402.5 (11.11)

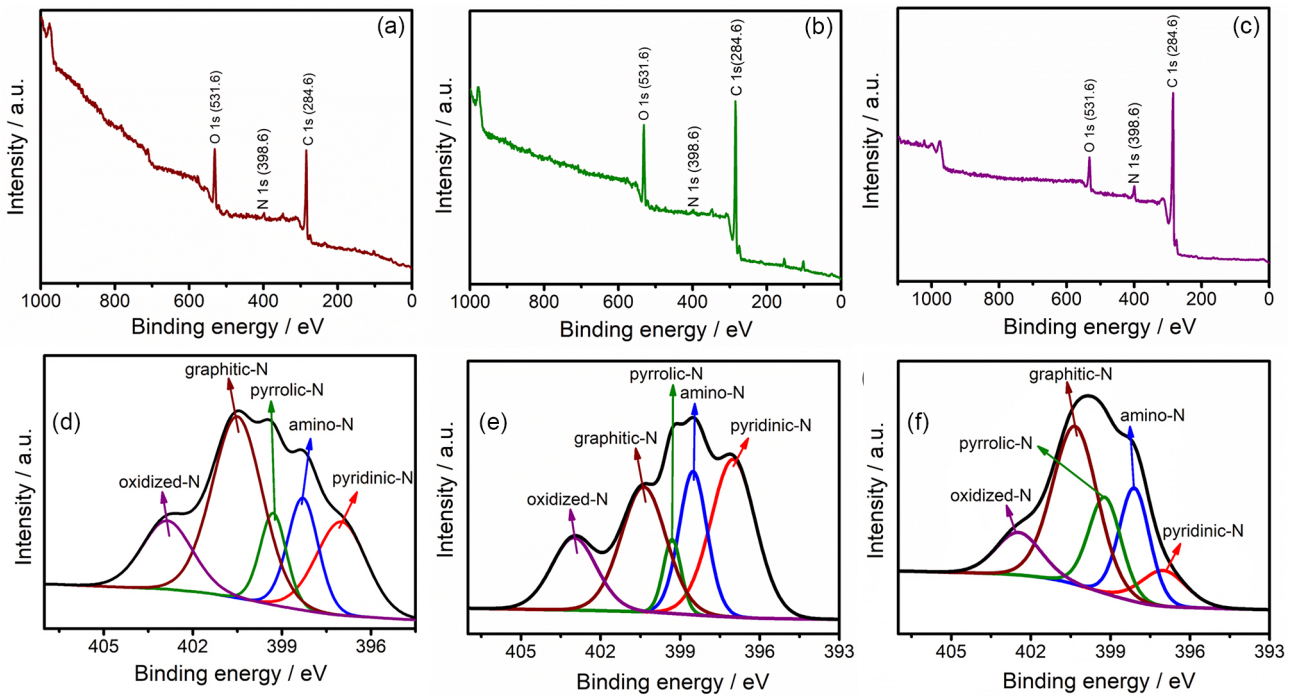

Figure 1. XPS survey spectra of (a) NrGO(1 – 1) 700, (b) NrGO(1 – 2) 700 and (c) NrGO(1 – 4) 700. High-resolution N 1s spectra of (d) NrGO(1 – 1) 700, (e) NrGO(1 – 2) 700 and (f) NrGO(1 – 4) 700.

In a recent report,[35] we demonstrated that incorporating nitrogen atoms into reduced graphene oxide sheets decreased the energies of the frontier orbitals, facilitating the polarization of CO_2 and resulting in improved solid-gas interactions. Theoretical experiments indicated that pyridinic-N and graphitic-N are the most effective species for CO_2 adsorption due to their higher solid-gas interaction strength. Additionally, amino groups can react with CO_2 to form carbamate species.[16,48,49] Thus, the high content of amino, pyridinic-N and graphitic-N species suggests that NrGO(1 – X)700 materials could be potential adsorbents for CO_2 capture.

ATR-FTIR spectra of graphite, GO and the intermediates NrGO(1 – 1), NrGO(1 – 2), NrGO(1 – 4) are presented in Figure S1 (Supplementary Information (SI) section). The graphite spectrum exhibited a band at 1546 cm^{-1}, attributed to C=C stretching. The GO spectrum showed bands at 3532 and 1621 cm^{-1} ascribed to O–H bond related to hydroxyl groups and water molecules.[50] Bands at 1725, 1220 and 1057 cm^{-1} were attributed to carboxylic, epoxide and alkoxy functional groups, confirming the oxidation of graphite flakes. In the spectra of NrGO(1 – 1), NrGO(1 – 2) and NrGO(1 – 4) the bands at 3346, 3283 and 1546 cm^{-1} were attributed to ν_s(N–H), ν_{as}(N–H), and δ(N–H), respectively, confirming the presence of amino groups. For the activated materials, the absence of bands related to amino and oxygen-based functional groups in the spectra of NrGO(1 – X)700 suggested the decomposition of DETA and oxygen functional groups during the activation process (Figure 2a). The decomposition of DETA resulted in the incorporation of nitrogen atoms into graphene structures, as demonstrated by XPS spectroscopy.

Raman spectra of NrGO(1 – X) displayed a D-band around 1360 cm^{-1}, attributed to the E_{2g} phonon of C sp^2 atoms, and a G-band at 1590 cm^{-1} attributed to A_{1g} breathing mode, as shown in Figure 2b.[51,52] The I_D/I_G ratio, which provides a measure of defects in the sp^2 domain, increased from graphite (0.131) to GO (0.947), as demonstrated in Figure S2 (SI section). This increase is due to the introduction of oxygen functional groups

during the oxidation reaction. The I_D/I_G ratios for the intermediate materials (before activation with K_2CO_3 at 700 °C), NrGO(1 – 1), NrGO(1 – 2), and NrGO(1 – 4) were 1.105, 1.100 and 1.103, respectively, higher than that of GO due to the presence of DETA (Figure S2). The activated materials showed even higher I_D/I_G values, e.g., NrGO(1 – 1)700 (1.115), NrGO(1 – 2)700 (1.157), and NrGO(1 – 4)700 (1.139), indicating an enhancement in defects caused by the introduction of nitrogen atoms into the graphene network and the removal of carbon atoms during the activation process.

PXRD patterns are shown in Figure S3 (SI section). Graphite flakes exhibited a strong basal diffraction at 2θ = 26.3º attributed to the plane (002), corresponding to a *d*-spacing of 3.38 Å. A second peak at 2θ = 54.4º was related to the plane (004).[15] In the case of GO, the (002) peak shifted to 2θ = 9.8º corresponding to a *d*-spacing of 9.01 Å. This increased *d*-spacing in GO, compared to graphite, was due to the presence of oxygen-containing functional groups and water molecules between carbon sheets.[53] PXRD patterns for NrGO(1 – X)700 exhibited a broad peak at 2θ = 23.0º (*d*-spacing = 3.83 Å), indicating a partial π-π restacking due to the removal oxygen-containing functional groups during the activation process (Figure 3a).

The nitrogen (N_2) adsorption and desorption isotherms obtained for NrGO(1 – 1)700, NrGO(1 – 2)700, and NrGO(1 – 4)700, collected at −196 °C, are displayed in Figures 3b-3d. The materials exhibited a combination of type I and type IV profiles, according to the International Union of Pure and Applied Chemistry (IUPAC) classification.[54] The initial part of the isotherms ($P/P_0 < 0.2$ bar) presented a concave curve characteristic of microporous materials and type I classification. In the range of $0.5 < P/P_0 < 1$ bar, the isotherms displayed an H2-type hysteresis loop typical of bottle-like pore network. This hysteresis is attributed to the difference in the N_2 condensation and evaporation phenomena. The specific surface areas S_{BET} were calculated using Brunauer-Emmet-Teller (BET) model, pore volumes and pore size distributions (Figure 3e) were obtained by Barret-Joyner-Halenda (BJH) method. The S_{BET} values were 283.47, 310.32, and 280.16 $m^2\ g^{-1}$ for NrGO(1 – 1)700, NrGO(1 – 2)700, and (1 – 4)700, respectively (Table 2). During the activation process, K_2CO_3 attacks both DETA and graphene structures. A slight increase in S_{BET} and pore volumes was observed from NrGO(1 – 1)700 to NrGO(1 – 2)700. However, this trend was not observed for NrGO(1 – 4)700, most likely because the amount of K_2CO_3 used mainly reacted with DETA, resulting in lower S_{BET} and pore volume for this material.

SEM image of GO revealed a bidimensional structure containing stacked sheets with a wrinkled morphology (Figure 3f). Comparing GO and NrGO(1 – X)700, SEM images of all NrGO(1 – X)700 exhibited three-dimensional porous structures, composed of highly crumpled and interconnected GO sheets (Figures 3g-3i). The holes observed in the NrGO(1 – X)700 structures were introduced by the activation process with K_2CO_3 during syntheses.

CO_2 adsorption studies

Isotherms were conducted at 25 °C to evaluate the CO_2 adsorption capacities of the NrGO(1 – X)700 materials (Figure 4). At 1 bar, the CO_2 capacities were 1.21, 2.00 and 4.60 mmol g^{-1} for NrGO(1 – 1)700, NrGO(1 – 2)700 and NrGO(1 – 4)700, respectively. Given that the specific surface areas, pore volumes and pore size distributions of NrGO(1 – X)700 were very similar, the higher capacity exhibited by NrGO(1 – 4)700 might be attributed to the stronger physical interactions between nitrogen functional groups present in this material and CO_2 molecules (Table 2). Moreover, NrGO(1 – 4)700 demonstrated higher CO_2 adsorption than other porous solids based on graphene,[15,18,55] carbon microporous materials,[57-59,61-63] and silica functionalized with amino group[16,17,60] reported in the literature, as indicated in Table 2.

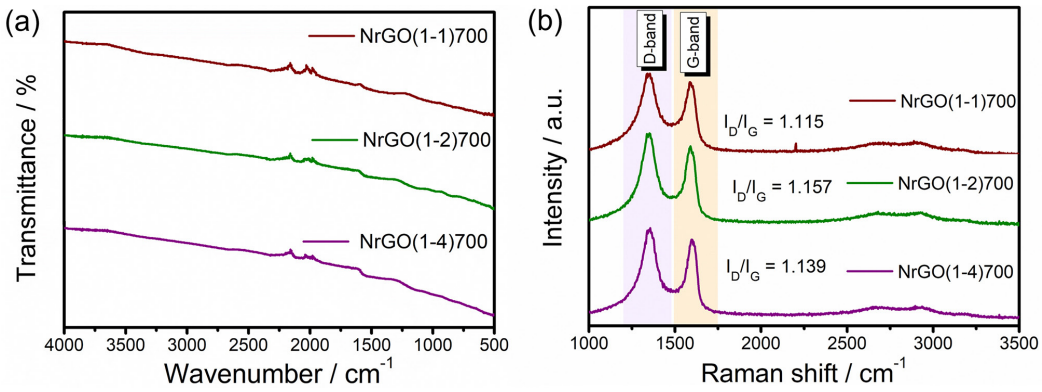

Figure 2. (a) ATR-FTIR and (b) Raman spectra for NrGO(1 – X)700.

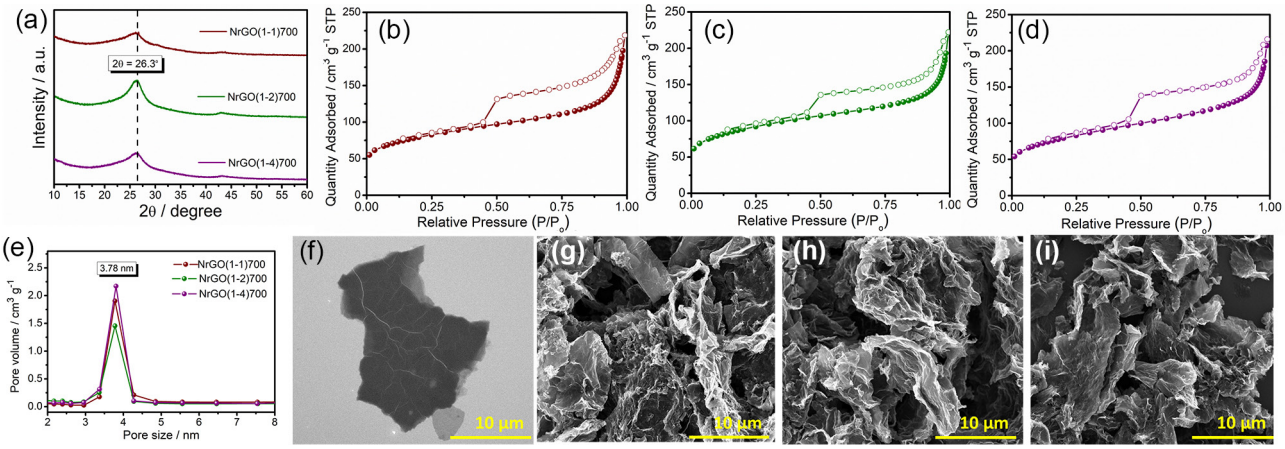

Figure 3. (a) PXRD patterns obtained for NrGO(1 – X)700. Nitrogen isotherms for (b) NrGO(1 – 1)700, (c) NrGO(1 – 2)700 and (d) NrGO(1 – 4)700 (open cycles for adsorption branch and empty cycles for desorption branches). (e) Pore size distributions for NrGO(1 – X)700 obtained from BJH method. Scanning electron microscopy (SEM) images for (f) GO, (g) NrGO(1 – 1)700, (h) NrGO(1 – 2)700 and (i) NrGO(1 – 4)700.

Table 2. Textural properties of the NrGO(1 – X)700, nitrogen contents and CO_2 capacities in comparison with other adsorbents in the literature

	Sample	S_{BET} / (m^2 g^{-1})	V_{Total} / (cm^3 g^{-1})	Pore size / nm	N / wt.%	S / wt.%	CO_2 uptake[a] / (mmol g^{-1})	Reference
Porous solids based on graphene	NrGO(1 – 1)700	283.47	0.305	3.78	3.39[b]/4.13[c]	–	1.21	this work
	NrGO(1 – 2)700	310.32		3.78	3.18[b]/3.43[c]	–	2.00	this work
	NrGO(1 – 4)700	280.16		3.78	3.59[b]/5.58[c]	–	4.60	this work
	a-RGO-950	1315.98	1.07	–	–	–	3.06	Chowdhury *et al.*[18]
	a-GDC-2	3240	2.23	2.75	–	–	2.0	Ganesan *et al.*[55]
	MEGO-I	310	0.94	2.4	–	–	0.85	dos Santos *et al.*[15]
Carbon microporous materials activated carbon	MNSM-700-2	1604	0.66	< 1	2.62	–	4.35	Bai *et al.*[56]
	CSC-750-0.5	1177	0.52	< 1	0.26	–	4.15	Bai *et al.*[57]
	CSPT-700-1	1188	0.47	< 1	0.27	7.07	3.59	Bai *et al.*[58]
	PPSC-650–2	1094	0.46	< 1	0.22	4.68	3.64	Bai *et al.*[59]
Silica functionalized with amino group	MCM-41-NH2	17	0.04	–	3.47	–	1.01	Mello *et al.*[17]
	MCM-41-N3	266	0.24	< 2.0	3.50	–	1.01	dos Santos *et al.*[16]
	W-AG-150A	73.1	0.31	12.5	5.12	–	1.97	Anyanwu *et al.*[60]

[a]CO_2 uptake: obtained at 25° C and 1 bar; [b]data obtained from elemental analyses; [c]data obtained from Survey XPS experiments. S_{BET}: specific surface area calculated by the BET method; V_{Total}: total pore volume, pore size distributions were determined by the Barrett-Joyner-Halenda (BJH).

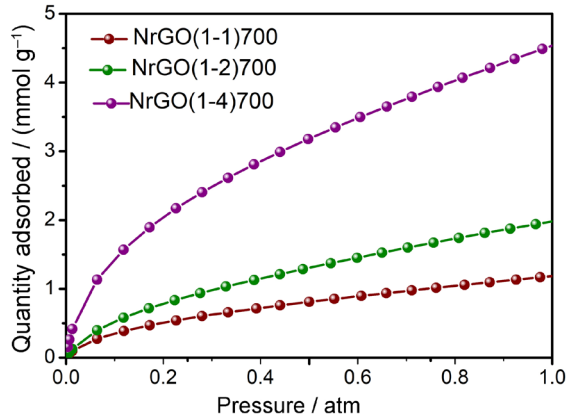

Figure 4. CO_2 isotherms obtained for NrGO(1 – X)700 obtained at 25 °C.

To investigate the interactions between NrGO(1 – X)700 and CO_2, we recorded their DRIFTS spectra after CO_2 adsorption. Before the experiments, the samples were heated to 100 °C under He flow for 1 h to remove adsorbed species. The CO_2 adsorption stage was performed at room temperature by introducing a CO_2 flow for 15 min. After stopping the CO_2 flow, the spectra were recorded (Figure 5a). The band at 2350 cm^{-1} was ascribed to the asymmetric stretching mode of CO_2 in the gas phase and physically adsorbed gas. The bands at 3630 and 3730 cm^{-1} were related to the combinations of $(2\nu_2 + \nu_3)$ and $(\nu_1 + \nu_3)$, respectively.[64] To understand the differences among the materials regarding the strength of solid-gas interaction, a CO_2 desorption experiment was conducted, at room

temperature. Under a He flow (15 mL min^{-1}), DRIFTS spectra were recorded every 2 min, and the area of the band at 2350 cm^{-1} was used to estimate the parameter λ (Figure S4-S6, SI section). The λ parameter was calculated by the ratio between the area of the band at 2350 cm^{-1} obtained at 0 min, and the area of the same band obtained at different times under He flow (desorption step). The values of λ parameter are shown in Table S1 (SI section). The plot of λ as function of desorption time is shown in Figure 5b. Comparing the values of λ parameter, we observed that NrGO(1 – 2)700 exhibited the highest tendency in the increase of the λ value, while NrGO(1 – 4)700 presented the lowest tendency. The λ parameters indicate that the strongest solid-gas interaction occurs for NrGO(1 – 4)700, and the weakest is for NrGO(1 – 2)700. In a recent report, we demonstrated from theoretical and experimental results that pyridinic and graphitic nitrogen atoms were more efficient for CO_2 capture than pyrrolic nitrogen.[35] The interaction involving pyridinic-N and CO_2 results from the nitrogen lone pair that attacks CO_2 molecule. Pyrrolic-N presents weak interactions with CO_2 because the lone pair of the nitrogen atom is committed in the conjugated π-system of the pyrrolic ring. Graphitic-N is also efficient for CO_2 adsorption because graphitic *meta*-N-doped can efficiently polarize CO_2 molecules,

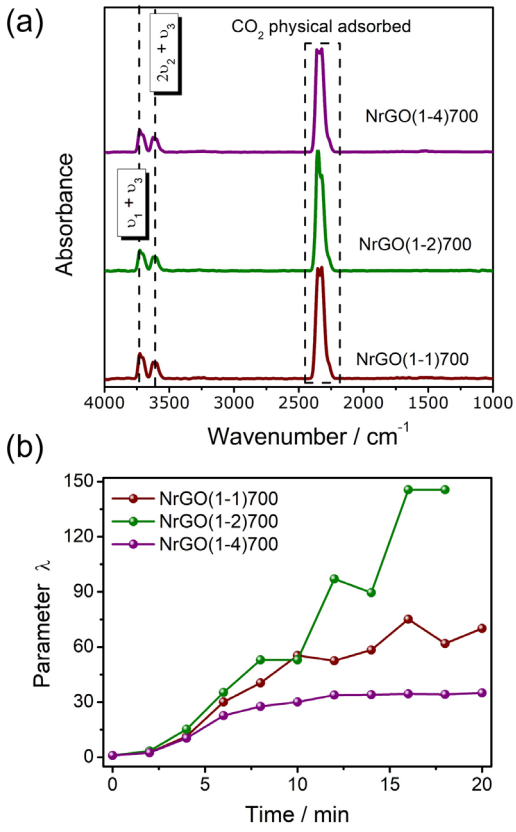

Figure 5. (a) DRIFTS spectra obtained after CO_2 adsorption on NrGO(1 – X)700. (b) Plot of parameter λ *versus* CO_2 desorption time.

favoring solid-gas interactions. Additionally, amino groups also present lone pairs to attack CO_2 molecules.[65] Table 1 shows the percentage of different types of nitrogen atoms in the NrGO(1 – X)700. Among the materials, NrGO(1 – 4)700 showed the highest percentage of amino groups and graphitic-N, suggesting that the strongest solid-gas interactions are expected. Most likely, the presence of the highest percentage of the amino and graphitic nitrogen within the micro and mesopores in NrGO(1 – 4)700 allows for the highest CO_2 adsorption for this solid. Therefore, in the nitrogen-doped graphene materials with similar textural properties, the results indicate a tendency for the increase of CO_2 adsorption with the increase of the percentages of amino groups and graphitic nitrogen in their structures.

Conclusions

This study successfully synthesized three porous adsorbent solids based on reduced graphene oxide using GO and DETA as precursors and K_2CO_3 as an activating agent. XPS analysis confirmed the incorporation of various nitrogen functionalities (pyridinic-N, amino, pyrrolic-N, graphitic-N and oxidized-N) into the adsorbent networks. N_2 isotherms showed that the NrGO(1 – X)700 series consisted of a mixture of micro and mesopores. CO_2 isotherms highlighted that NrGO(1 – 4)700 exhibited the highest CO_2 adsorption capacity, likely due to its higher percentage of amino groups and graphitic nitrogen. DRIFTS experiments indicated that NrGO(1 – 4)700 possesses the strongest solid-gas interactions. This is attributed to its high content of amino groups and graphitic nitrogen, which induce strong interactions with CO_2, resulting in superior CO_2 adsorption. Thus, the CO_2 adsorption capacity of nitrogen-doped adsorbents based on reduced graphene oxide, with similar values of textural properties (specific surface area, pore volume and pore size) increases with the amount of amino groups and graphitic nitrogen. This investigation not only highlights the synthesis of cost-effective and environmentally CO_2 adsorbent materials from graphite but also positions NrGO(1 – 4)700 as a viable material for efficient CO_2 capture in low-pressure applications, marking a significant stride towards addressing global carbon capture challenges.

Supplementary Information

Supplementary information (ATR-FTIR, Raman spectra and PXRD patterns of GO, graphite, NrGO(1 – 1), NrGO(1 – 2) and NrGO(1 – 4); *in situ* DRIFTS spectra of CO_2 desorption on the NrGO(1 – X)700 sample as

a function of time during helium purge; evaluation of CO_2 desorption with time in helium purge in DRIFTS analysis through parameter λ) is available free of charge at http://jbcs.sbq.org.br as PDF file.

Acknowledgments

This work was supported by the Brazilian agencies Conselho Nacional de Desenvolvimento Científico e Tecnológico (CNPq), Coordenação de Aperfeiçoamento de Pessoal de Nível Superior (CAPES), Programa Institucional de Bolsas de Iniciação Científica (PIBIC) and Fundação Carlos Chagas Filho de Amparo à Pesquisa do Estado do Rio de Janeiro (FAPERJ). We are grateful to Laboratórios Multiusuário de Caracterização de Materiais e Espectroscopia Molecular from Universidade Federal Fluminense.

Author Contributions

Matheus G. Ribeiro was responsible for investigation, writing original draft, formal analysis; Isabela A. A. Bessa, Aline F. M. da Silva, Carolina B. P. Ligiero, Leonardo O. Osta, Ludmila P. C. Silva for investigation, writing original draft, review and editing, formal analysis; Joyce R. Araujo for data curation; Bráulio S. Archanjo for support with MEV experiments; Célia M. Ronconi, Thiago C. dos Santos for conceptualization, data curation, formal analysis, funding acquisition, project administration, resources, writing original draft, review and editing.

References

1. de Araujo, I. L.; Costa, H. K. M.; Makuch, Z.; *Ambient. Soc.* **2022**, *25*. [Crossref]
2. Xu, D.; Bisht, G.; Tan, Z.; Sinha, E.; Di Vittorio, A. V.; Zhou, T.; Ivanov, V. Y.; Leung, L. R.; *Nat. Commun.* **2024**, *15*, 2438. [Crossref]
3. Obame-Nkoghe, J.; Agossou, A. E.; Mboowa, G.; Kamgang, B.; Caminade, C.; Duke, D. C.; Githeko, A. K.; Ogega, O. M.; Engone Elloué, N.; Sarr, F. B.; Nkoghe, D.; Kengne, P.; Ndam, N. T.; Paupy, C.; Bockarie, M.; Voua Otomo, P.; *Infect. Diseases Poverty* **2024**, *13*, 26. [Crossref]
4. Ribeiro, M. G.; Hisse, D.; Prado, M. L.; dos Santos, T. C.; Ronconi, C. M.; *Rev. Virtual Quim.* **2022**, *14*, 517. [Crossref]
5. Chagas, J. A. O.; Marciniak, A. A.; Mota, C. J. A.; *J. Braz. Chem. Soc.* **2022**, *33*, 801. [Crossref]
6. Zhang, K.; Wang, R.; *Chem. Eng. J.* **2024**, *485*, 149495. [Crossref]
7. dos Santos, T. C.; Lage, M. R.; da Silva, A. F. M.; Fernandes, T. S.; Carneiro, J. W. M.; Ronconi, C. M.; *J. CO_2 Util.* **2022**, *61*, 102054. [Crossref]
8. Sang Sefidi, V.; Luis, P.; *Ind. Eng. Chem. Res.* **2019**, *58*, 20181. [Crossref]
9. de Vasconcelos, S. F.; Carneiro, L. O.; Brito, R. P.; Brito, K. D.; *J. Braz. Chem. Soc.* **2023**, *34*, 441. [Crossref]
10. Pirouzmand, M.; Nikzad-Kojanag, B.; Hosseini-Yazdi, S. A.; *J. Braz. Chem. Soc.* **2016**, *27*, 2354. [Crossref]
11. Dinda, S.; *Mater. Today Commun.* **2023**, *35*, 105927. [Crossref]
12. Oliveira, D. E. F.; Chagas, J. A. O.; de Lima, A. L.; Mota, C. J. A.; *Ind. Eng. Chem. Res.* **2022**, *61*, 10522. [Crossref]
13. Najafi, A. M.; Soltanali, S.; Khorashe, F.; Ghassabzadeh, H.; *Chemosphere* **2023**, *324*, 138275. [Crossref]
14. Sunny, K. S. F.; Felipe, L. O.; Thiago, C. S.; Danilo, H.; Claudia, M.; Ronconi, C. M.; Pierre, M. E.; *Chem.-Eur. J.* **2020**, *27*, 2342. [Crossref]
15. dos Santos, T. C.; Ronconi, C. M.; *J. CO_2 Util.* **2017**, *20*, 292. [Crossref]
16. dos Santos, T. C.; Bourrelly, S.; Llewellyn, P. L.; Carneiro, J. W. M.; Ronconi, C. M.; *Phys. Chem. Chem. Phys.* **2015**, *17*, 11095. [Crossref]
17. Mello, M. R.; Phanon, D.; Silveira, G. Q.; Llewellyn, P. L.; Ronconi, C. M.; *Microporous Mesoporous Mat.* **2011**, *143*, 174. [Crossref]
18. Chowdhury, S.; Balasubramanian, R.; *Ind. Eng. Chem. Res.* **2016**, *55*, 7906. [Crossref]
19. Barbosa, M. N.; Costa, M. J. F.; Barbosa, M. N.; Júnior, V. J. F.; Salazar-Banda, G. R.; Reyes-Carmona, Á.; Rodríguez-Castellón, E.; Araujo, A. S.; *Rev. Matéria* **2021**, *26*, e13085. [Crossref]
20. Liu, Z. J.; Zhang, W. H.; Yin, M. J.; Ren, Y. H.; An, Q. F.; *Sep. Purif. Technol.* **2023**, *312*, 123448. [Crossref]
21. Chagas, J. A. O.; Crispim, G. O.; Pinto, B. P.; San Gil, R. A. S.; Mota, C. J. A.; *ACS Omega* **2020**, *5*, 29520. [Crossref]
22. Hisse, D.; Bessa, I. A. A.; Silva, L. P. C.; da Silva, A. F. M.; Araujo, J. R.; Archanjo, B. S.; Soares, A. V. H.; Passos, F. B.; Carneiro, J. W. M.; dos Santos, T. C.; Ronconi, C. M.; *J. Braz. Chem. Soc.* **2024**, *35*, e-20240034. [Crossref]
23. Soylak, M.; Ozalp, O.; Uzcan, F.; *Trends Environ. Anal. Chem.* **2021**, *29*, e00109. [Crossref]
24. Jagirani, M. S.; Soylak, M.; *Microchem. J.* **2020**, *159*, 105436. [Crossref]
25. Serodre, T.; Oliveira, N. A. P.; Miquita, D. R.; Ferreira, M. P.; Santos, A. P.; Resende, V. G.; Furtado, C. A.; *J. Braz. Chem. Soc.* **2019**, *30*, 2488. [Crossref]
26. Drashya; Lal, S.; Hooda, S.; *AIP Conf. Proc.* **2018**, *1953*, 334. [Crossref]
27. Peigney, A.; Laurent, C.; Flahaut, E.; Bacsa, R. R.; Rousset, A.; *Carbon* **2001**, *39*, 507. [Crossref]
28. Kamedulski, P.; Skorupska, M.; Binkowski, P.; Arendarska, W.; Ilnicka, A.; Lukaszewicz, J. P.; *Sci. Rep.* **2021**, *11*, 22054. [Crossref]

29. Karaman, C.; Bayram, E.; Karaman, O.; Aktaş, Z.; *J. Electroanal. Chem.* **2020**, *868*, 114197. [Crossref]
30. Ruhaimi, A. H.; Hitam, C. N. C.; Aziz, M. A. A.; Hamid, N. H. A.; Setiabudi, H. D.; Teh, L. P.; *Renewable Sustainable Energy Rev.* **2022**, *167*, 112840. [Crossref]
31. Ren, L.; Hui, K. N.; Hui, K. S.; Liu, Y.; Qi, X.; Zhong, J.; Du, Y.; Yang, J.; *Sci. Rep.* **2015**, *5*, 14229. [Crossref]
32. Nie, L.; Li, S.; Cao, M.; Han, N.; Chen, Y.; *J. Environ. Sci.* **2025**, *149*, 209. [Crossref]
33. Mercier, G.; Klechikov, A.; Hedenstrom, M.; Johnels, D.; Baburin, I. A.; Seifert, G.; Mysyk, R.; Talyzin, A. V.; *J. Phys. Chem. C* **2015**, *119*, 27179. [Crossref]
34. Xie, Y.; Wang, X.; Hou, L.; Wang, X.; Zhang, Y.; Zhu, C.; Hu, Z.; He, M.; *J. Energy Storage* **2021**, *38*, 102530. [Crossref]
35. dos Santos, T. C.; Mancera, R. C.; Rocha, M. V. J.; da Silva, A. F. M.; Furtado, I. O.; Barreto, J.; Stavale, F.; Archanjo, B. S.; Carneiro, J. W. M.; Costa, L. T.; Ronconi, C. M.; *J. CO_2 Util.* **2021**, *48*, 101517. [Crossref]
36. Gao, B.; Feng, X.; Zhang, Y.; Zhou, Z.; Wei, J.; Qiao, R.; Bi, F.; Liu, N.; Zhang, X.; *Chem. Eng. J.* **2024**, *484*, 149604. [Crossref]
37. Chen, Y.; Zhong, C.; Wu, J.; Ma, J.; Yu, X.; Liu, Y.; *Langmuir* **2022**, *38*, 14192. [Crossref]
38. Storck, S.; Bretinger, H.; Maier, W. F.; *Appl. Catal., A* **1998**, *174*, 137. [Crossref]
39. Mukhtar, A.; Saqib, S.; Mellon, N. B.; Babar, M.; Rafiq, S.; Ullah, S.; Bustam, M. A.; Al-Sehemi, A. G.; Muhammad, N.; Chawla, M.; *J. Nat. Gas Sci. Eng.* **2020**, *77*, 103203. [Crossref]
40. Yang, Z.; Yuan, B.; Clarkson, C. R.; Ghanizadeh, A.; *Fuel* **2021**, *285*, 118974. [Crossref]
41. Younas, M.; Rezakazemi, M.; Daud, M.; Wazir, M. B.; Ahmad, S.; Ullah, N.; Inamuddin; Ramakrishna, S.; *Prog. Energy Combust. Sci.* **2020**, *80*, 100849. [Crossref]
42. Vitorino, L. S.; dos Santos, T. C.; Bessa, I. A. A.; Santos, E. C. S.; Verçoza, B. R. F.; de Oliveira, L. A. S.; Rodrigues, J. C. F.; Ronconi, C. M.; *Colloids Surf., B* **2022**, *209*, 112169. [Crossref]
43. dos Santos, T. C.; Santos, E. C. S.; Dias, J. P.; Barreto, J.; Stavale, F. L.; Ronconi, C. M.; *Fuel* **2019**, *256*, 115793. [Crossref]
44. Hummers, W. S.; Offeman, R. E.; *J. Am. Chem. Soc.* **1958**, *80*, 1339. [Crossref]
45. *CasaXPS*, version 2.3.19; Casa Software Ltd., Teignmouth, UK, 2018.
46. Khan, M. H.; Akash, N. M.; Akter, S.; Rukh, M.; Nzediegwu, C.; Islam, M. S.; *J. Environ. Manage.* **2023**, *338*, 117825. [Crossref]
47. Hussin, F.; Kiat, L. B.; Yusoff, R.; Aroua, M. K.; *Environ. Eng. Res.* **2024**, *29*, 230005. [Crossref]
48. Rim, G.; Priyadarshini, P.; Song, M. G.; Wang, Y.; Bai, A.; Realff, M. J.; Lively, R. P.; Jones, C. W.; *J. Am. Chem. Soc.* **2023**, *145*, 7190. [Crossref]
49. Shimon, D.; Chen, C. H.; Lee, J. J.; Didas, S. A.; Sievers, C.; Jones, C. W.; Hayes, S. E.; *Environ. Sci. Technol.* **2018**, *52*, 1488. [Crossref]
50. Helmi, M.; Farahani, Z. K.; Hemmati, A.; Ghaemi, A.; *Sci. Rep.* **2024**, *14*, 5511. [Crossref]
51. Xia, K.; Tian, X.; Fei, S.; You, K.; *Int. J. Hydrogen Energy* **2014**, *39*, 11047. [Crossref]
52. Zhang, H.; Bhat, V. V.; Gallego, N. C.; Contescu, C. I.; *ACS Appl. Mater. Interfaces* **2012**, *4*, 3239. [Crossref]
53. Shabil Sha, M.; Anwar, H.; Musthafa, F. N.; Al-Lohedan, H.; Alfarwati, S.; Rajabathar, J. R.; Khalid Alahmad, J.; Cabibihan, J. J.; Karnan, M.; Kumar Sadasivuni, K.; *Sci. Rep.* **2024**, *14*, 3608. [Crossref]
54. Thommes, M.; Kaneko, K.; Neimark, A. V.; Olivier, J. P.; Rodriguez-Reinoso, F.; Rouquerol, J.; Sing, K. S. W.; *Pure Appl. Chem.* **2015**, *87*, 1051. [Crossref]
55. Ganesan, A.; Shaijumon, M. M.; *Microporous Mesoporous Mat.* **2016**, *220*, 21. [Crossref]
56. Bai, J.; Huang, J.; Yu, Q.; Demir, M.; Kilic, M.; Altay, B. N.; Hu, X.; Wang, L.; *Fuel Process. Technol.* **2023**, *249*, 107854. [Crossref]
57. Bai, J.; Huang, J.; Yu, Q.; Demir, M.; Akgul, E.; Altay, B. N.; Hu, X.; Wang, L.; *Front. Chem. Sci. Eng.* **2023**, *17*, 1122. [Crossref]
58. Bai, J.; Shao, J.; Yu, Q.; Demir, M.; Nazli Altay, B.; Muhammad Ali, T.; Jiang, Y.; Wang, L.; Hu, X.; *Chem. Eng. J.* **2024**, *479*, 147667. [Crossref]
59. Bai, J.; Huang, J.; Jiang, Q.; Jiang, W.; Demir, M.; Kilic, M.; Altay, B. N.; Wang, L.; Hu, X.; *Colloids Surf., A* **2023**, *674*, 131916. [Crossref]
60. Anyanwu, J. T.; Wang, Y.; Yang, R. T.; *Ind. Eng. Chem. Res.* **2020**, *59*, 7072. [Crossref]
61. Li, W.; Tu, W.; Cheng, J.; Yang, F.; Wang, X.; Li, L.; Shang, D.; Zhou, X.; Yu, C.; Yuan, A.; Pan, J.; *Sep. Purif. Technol.* **2022**, *282*, 120001. [Crossref]
62. Adio, S. O.; Ganiyu, S. A.; Usman, M.; Abdulazeez, I.; Alhooshani, K.; *Chem. Eng. J.* **2020**, *382*, 122964. [Crossref]
63. Gan, F.; Wang, B.; Guo, J.; He, J.; Ma, S.; Jiang, X.; Jin, Z.; *Sep. Purif. Technol.* **2022**, *302*, 122089. [Crossref]
64. Danon, A.; Stair, P. C.; Weitz, E.; *J. Phys. Chem. C* **2011**, *115*, 11540. [Crossref]
65. Furtado, I. O.; dos Santos, T. C.; Vasconcelos, L. F.; Costa, L. T.; Fiorot, R. G.; Ronconi, C. M.; Carneiro, J. W. M.; *Chem. Eng. J.* **2021**, *408*, 128002. [Crossref]

Submitted: February 25, 2024
Published online: May 29, 2024